

# Supplement

## Measurement report: Radiative efficiency estimates of $(\text{CF}_3)_2\text{CFCN}$ , $\text{CF}_3\text{OCFCF}_2$ , and $\text{CF}_3\text{OCF}_2\text{CF}_3$ using high-resolution Fourier transform infrared spectroscopy

Beni Adi Trisna, Seungnam Park<sup>†</sup>, Injun Park<sup>††</sup>, Jeongsoon Lee\*, Jeong Sik Lim\*

Greenhouse Gas Metrology team, Korea Research Institute of Standard and Science (KRISS)

Science of Measurement, University of Science and Technology (UST)

<sup>†</sup>National Center of Standard Reference Data (NCSRD), Korea Research Institute of Standard and Science (KRISS)

<sup>††</sup>Interface Materials and Chemical Engineering Research Center, Korea Research Institute of Chemical Technology

### CONTENTS

S1. Curve-of-growth measurement for OPL calibration of MP

S2. Uncertainties of fitted peak area and COG slope

S3. Parametric evaluation of uncertainty of RE

Fig. S1. ILS reconstruction results from the  $\text{N}_2\text{O}$  spectrum measurement

Fig. S2. Responsivity drift measurement

Table S1. Uncertainty budget of OPL calibration of MP

Table S2. Referred line data for OPL calibration of MP

Table S3. Uncertainty budget of RE value of  $\text{NF}_3$

Table S4. Uncertainty budget of RE value of  $\text{SF}_6$

Table S5. Uncertainty budget of RE value of  $\text{CF}_4$

Table S6. Uncertainty budget of RE value of PMVE

Table S7. Uncertainty budget of RE value of PFMEE

## ST 1. Curve-of-growth measurement for OPL calibration of MP

The N<sub>2</sub>O in N<sub>2</sub> mixture flowed to the MP at different N<sub>2</sub>O partial pressures ranging between 0.0015 and 0.048 Torr. The mixture was prepared by mixing a high purity N<sub>2</sub>O (99.9999%) with a high purity N<sub>2</sub> (99.9999%) using a precision gas mixer (Sonimix 2106). The mixing ratio of N<sub>2</sub>O was set at  $0.07969 \pm 0.00016$  cmol/mol. The gas mixture filled the cell between 1.9 and 60.1 Torr which was measured using a calibrated pressure gauge (MKS 626A13TBE). The data acquisition parameters were the same as those used for the OPL calibration measurements (Table 1). The only exception was the size of the aperture, which was set at 4 mm to increase the SNR at lower partial pressure measurements.

Absorption spectra were recorded at various N<sub>2</sub>O partial pressures. The spectral absorption  $A(\tilde{\nu})$  is  $-\ln(\Phi(\tilde{\nu})/\Phi_0(\tilde{\nu}))$ , where  $\Phi(\tilde{\nu})$  and  $\Phi_0(\tilde{\nu})$  are the transmitted and incident radiant powers, respectively. Subsequently, the ILS were deconvoluted by applying the ILS deconvolution procedure using home-written code, namely multispectrum fitting. In this code, the nonlinear least-squares (NLS) method was applied. The model function was the Voigt profile (VP) defined by  $V(\tilde{\nu}, \mathbf{a})$  with the coefficient vector  $\mathbf{a}$  consisting of the transition wavenumber, peak intensity, Lorentzian width, and Doppler width. The model function of  $V(\tilde{\nu}, \mathbf{a})$  was convoluted with the instrument lineshape  $ILS(\tilde{\nu})$  to simulate the modelled spectra. The model function of  $V(\tilde{\nu}, \mathbf{a})$  was rationally approximated from the real part of the complex probability function.<sup>1</sup> Then, the near-solution coefficient vector  $\mathbf{a}_0$  was determined by minimizing the residual quantity between the measured and modeled spectra. Because the closed-form solution of the sum of squared residuals (SSR) does not exist, the trust-region-reflective (TRR) algorithm serves to minimize the SSR.<sup>2</sup> The TRR algorithm forces global convergence (via the steepest descent or negative curvature direction) and achieves fast local convergence (via the Newton step when it exists).

After obtaining the best-fit parameters for each transition peak, that is, the optimized transition wavenumber, peak intensity, Lorentzian width, and Doppler width, the pure gas spectrum  $A_{pgs}(\tilde{\nu})$  was reconstructed from the optimized parameters.  $A_{pgs}(\tilde{\nu})$  for each partial pressure is shown in Figure 2 of the main text (left, second row), which is obtained from the convolution of the Lorentzian and Doppler widths. The area under the  $A_{pgs}(\tilde{\nu})$  was calculated using the trapezoidal rule:

$$\int_a^b f(x)dx \approx \sum_{k=1}^N \frac{f(x_{k-1})+f(x_k)}{2} \Delta x_k \quad (\text{S1})$$

where the  $\Delta x_k$  denotes the grid spacing of the data. The accuracy of this approximation depends on the grid resolution. Therefore, the grid resolution of the wavenumber is increased to 100,000 vector wavenumbers for each peak. Thus, the total wavenumber grid for the four peaks is 400,000. This method was validated by comparing the integration results with Origin's peak analyzer and the integration tool. A negligible difference ( $5.1 \times 10^{-6} \%$ ) was found between the two procedures.

## ST 2. Uncertainty evaluation of optical path length calibration

### *Derivation of uncertainty model equations*

The uncertainty of  $L_{MP}$  was estimated based on the general law of uncertainty propagation (LUP) using the model equation:

$$L_{MP} = \frac{T_{MP} \cdot P_{RC} \cdot L_{RC} \cdot A_{MP} \cdot S_{T,RC}}{T_{RC} \cdot P_{MP} \cdot A_{RC} \cdot S_{T,MP}} \quad (S2)$$

where  $T$ ,  $P$ ,  $L$ ,  $A$ , and  $S_T$  are the temperature, pressure, optical path length, absorption, and reference-line strength, respectively. The subscripts RC and MP represent the reference and multipass cells, respectively.

The line strengths of RC and MP are governed by the thermodynamic and quantum chemical properties of the molecules, which can be estimated by the following equation<sup>3</sup>:

$$S_T = \left( \frac{Q_{T_0}}{Q_T} \right) \cdot \exp \left\{ -h \cdot c \cdot \frac{E''}{k_B} \cdot \left( \frac{1}{T} - \frac{1}{T_0} \right) \right\} \cdot \frac{\left[ 1 - \exp \left\{ -h \cdot c \cdot \left( \frac{\tilde{\nu}_0}{k_B \cdot T} \right) \right\} \right]}{\left[ 1 - \exp \left\{ -h \cdot c \cdot \left( \frac{\tilde{\nu}_0}{k_B \cdot T_0} \right) \right\} \right]} \cdot S_0 = P_T \cdot S_0 \quad (S3)$$

where  $Q_{T_0}$  (5007.816 at standard temperature) and  $Q_T$  are the partition functions of the absorbing gas at a reference temperature  $T_0$  (296 K) and measured temperature  $T$ , respectively. where  $h$  is Planck's constant,  $E''$  is the ground state energy of the corresponding transition,  $\tilde{\nu}_0$  is the transition wavenumber, and  $c$  is the speed of light. Substituting eq S3 into eq S2 yields:

$$L_{MP} = \frac{T_{MP} \cdot P_{RC} \cdot L_{RC} \cdot A_{MP} \cdot P_{T,RC} \cdot S_0}{T_{RC} \cdot P_{MP} \cdot A_{RC} \cdot P_{T,MP} \cdot S_0} \quad (S4)$$

According to LUP, the combined standard uncertainty of the calibration result  $y$ , designated as  $u_c(y)$  is obtained from a first-order Taylor series approximation of  $y = f(X_1, X_2, \dots, X_N)$  which is given by<sup>4</sup>

$$u_c^2(y) = \sum_{i=1}^N \left( \frac{\partial f}{\partial x_i} \right)^2 u^2(x_i) + 2 \sum_{i=1}^{N-1} \sum_{j=1+1}^n \frac{\partial f}{\partial x_i} \frac{\partial f}{\partial x_j} u(x_i) \cdot u(x_j) \cdot \rho_{ij} \quad (S5)$$

where the terms regarding partial derivatives are sensitivity coefficients,  $u(x_i)$  is the standard uncertainty associated with input estimate  $x_i$ , and the term  $u(x_i) \cdot u(x_j) \cdot \rho_{ij}$  is the estimated covariance associated with input estimates  $x_i$  and  $x_j$  with Pearson correlation coefficient  $\rho_{ij}$ . In eq S1, only the reference line strength  $S_0$  is perfectly and positively correlated ( $\rho = 1$ ), whereas the other parameters are uncorrelated ( $\rho = 0$ ). Thus, eq S4 can be derived as:

$$\begin{aligned} u_c^2(L_{MP}) = & \left( \frac{\partial L_{MP}}{\partial T_{MP}} \right)^2 u^2(T_{MP}) + \left( \frac{\partial L_{MP}}{\partial P_{RC}} \right)^2 u^2(P_{RC}) + \left( \frac{\partial L_{MP}}{\partial L_{RC}} \right)^2 u^2(L_{RC}) + \\ & \left( \frac{\partial L_{MP}}{\partial A_{MP}} \right)^2 u^2(A_{MP}) + \left( \frac{\partial L_{MP}}{\partial P_{T,RC}} \right)^2 u^2(P_{T,RC}) + \left( \frac{\partial L_{MP}}{\partial S_{0,RC}} \right)^2 u^2(S_{0,RC}) + \left( \frac{\partial L_{MP}}{\partial T_{RC}} \right)^2 u^2(T_{RC}) + \\ & \left( \frac{\partial L_{MP}}{\partial P_{MP}} \right)^2 u^2(P_{MP}) + \left( \frac{\partial L_{MP}}{\partial A_{RC}} \right)^2 u^2(A_{RC}) + \left( \frac{\partial L_{MP}}{\partial P_{T,MP}} \right)^2 u^2(P_{T,MP}) + \left( \frac{\partial L_{MP}}{\partial S_{0,MP}} \right)^2 u^2(S_{0,MP}) + \\ & 2 \frac{\partial L_{MP}}{\partial S_{0,RC}} \frac{\partial L_{MP}}{\partial S_{0,MP}} u(S_{0,RC}) \cdot u(S_{0,MP}) \cdot \rho_{S_{0,RC} S_{0,MP}} \end{aligned} \quad (S6)$$

Because the line strengths of the probed reference lines  $S_0$  are the same for RC and MP, the uncertainties from  $S_0$  and the sensitivity coefficients were identical. The term  $S_{T,MP}$  ( $= P_{T,MP} \cdot S_0$ ) in the denominator of eq S1 results in a negative sensitivity coefficient, leading  $\frac{\partial L_{MP}}{\partial S_{0,RC}} = -\frac{\partial L_{MP}}{\partial S_{0,MP}}$ . Because the corresponding correlation coefficient is positive and perfect,  $\rho_{S_{0,RC} S_{0,MP}} = 1$ , the uncertainties of the reference line strengths  $S_0$  can be cancelled, namely  $\left( \frac{\partial L_{MP}}{\partial S_0} \right)^2 u^2(S_0) + \left( \frac{\partial L_{MP}}{\partial S_0} \right)^2 u^2(S_0) - 2 \frac{\partial L_{MP}}{\partial S_0} \frac{\partial L_{MP}}{\partial S_0} u(S_0) \cdot u(S_0) = 0$ . For the uncertainty due to the temperature-dependent prefactor  $P_T$ , although the sensitivity coefficients of RC and MP were the same, the extents of temperature variations of RC and MP were slightly different. Additionally, the measurements were independent ( $\rho = 0$ ). Thus, the uncertainty cannot be ignored. Hence, eq S6 becomes:

$$\begin{aligned}
u_c^2(L_{MP}) = & \left(\frac{\partial L_{MP}}{\partial T_{MP}}\right)^2 u^2(T_{MP}) + \left(\frac{\partial L_{MP}}{\partial P_{RC}}\right)^2 u^2(P_{RC}) + \left(\frac{\partial L_{MP}}{\partial L_{RC}}\right)^2 u^2(L_{RC}) + \\
& \left(\frac{\partial L_{MP}}{\partial A_{MP}}\right)^2 u^2(A_{MP}) + \left(\frac{\partial L_{MP}}{\partial P_{T,RC}}\right)^2 u^2(P_{T,RC}) + \left(\frac{\partial L_{MP}}{\partial T_{RC}}\right)^2 u^2(T_{RC}) + \left(\frac{\partial L_{MP}}{\partial P_{MP}}\right)^2 u^2(P_{MP}) + \\
& \left(\frac{\partial L_{MP}}{\partial A_{RC}}\right)^2 u^2(A_{RC}) + \left(\frac{\partial L_{MP}}{\partial P_{T,MP}}\right)^2 u^2(P_{T,MP})
\end{aligned} \tag{S7}$$

Then dividing eq S6 with  $L_{MP}^2$ , yields:

$$\begin{aligned}
ru^2(L_{MP}) = & ru^2(T_{MP}) + ru^2(P_{RC}) + ru^2(L_{RC}) + \\
& ru^2(A_{MP}) + ru^2(P_{T,RC}) + ru^2(T_{RC}) + ru^2(P_{MP}) + ru^2(A_{RC}) + ru^2(P_{T,MP})^2
\end{aligned} \tag{S8}$$

where  $ru$  denotes relative standard uncertainty, *e.g.*  $ru(y) = \frac{u(y)}{y}$ .

#### *Uncertainties of fitted peak area and COG slope*

In typical spectrum fitting, if the model function is appropriately selected and the minimizer finds the global minimum, the residuals are randomly distributed.<sup>5</sup> This causes the fit residuals to be distributed normally to be propagated toward the uncertainty of the fitted area and finally identical to a general case of parametric uncertainty evaluation with a known probability distribution function. In contrast, our result exhibited a W-shaped pattern in the residuals (Figure 1), implying unresolved systematic uncertainty. Based on the assumption that VP is the best lineshape function for the measured line and that the algorithm error is negligible at the minimized SSR, the uncertainty of the area of the absorption line  $u(A_{line})$  was regarded as a consequence of instrumental error (nonideal PE and ME), including the drift of the ILS. Therefore, uniform distribution with a boundary limited to the maximum deviation of the residuals should be applied to obtain the uncertainty value of the fitted area. Because a rectangular distribution results in the most conservative uncertainty among the known statistical distributions, this approach cannot underestimate the uncertainty of the fitted area.

The nonlinearities in the absorption area should be tested to determine a linearly responding regime to simplify the OPL calibration procedure. If comparison measurements are conducted in a linear region, OPL calibration can be accomplished by one-point calibration, that is, the ratio method. The N<sub>2</sub>O absorption burdens of RC and MP cells differed by 7.6 times as shown in Figure 2. The curve-of-growth measurements showed that

the RC and MP measurements were within the linear region (Figure 2). However, the slope determined by the weighted least squares method was uncertain due to regression uncertainty.<sup>5</sup> To account for this, the relative standard uncertainty of the slope in the curve-of-growth  $ru_{slope}$  was added to the uncertainty of the area of the MP cell  $ru_{AMP}$ . The slope of the straight line was  $6.96 \times 10^{-6}$ , while the expanded uncertainty of the slope was  $1.67 \times 10^{-7}$ .<sup>7</sup> Therefore, the estimated value of  $ru_{slope}$  is 1.2%. Finally, the uncertainties of the fitted area covering the measured four peaks were estimated to be  $ru_{ARC} = 0.13\%$  and  $ru_{AMP} = 1.2\%$ , respectively for the RC and the MP.

#### *Uncertainty of line strengths of N<sub>2</sub>O*

In the wavenumber range 2217.4 – 2219.0 cm<sup>-1</sup>, the rovibrational transitions belong to the common transition band of 1001←1000, yielding an identical value of  $E''$  for each transition. The details of the referred line data are summarized in Table S2. The partition function of N<sub>2</sub>O was taken from the HITRAN database, in which temperature and several partition functions resulted in a linear relationship of  $\Delta Q \cong 22.850 \cdot \Delta T$  in the range of 291–300 K. In our study, the cell temperature varied within  $297 \pm 1$  K and the probability distribution was assumed to be uniform. Therefore, the temperature-dependent prefactor  $P_T$  was evaluated based on the variation trend of the temperature and the resulting partition function term ( $\frac{Q_{T_0}}{Q_{T_0} + \Delta Q}$ ). The uncertainty of the reference line strength was cancelled according to eq S6. The line strength was varied by varying the temperature-dependent prefactor,  $P_T$ . The temperature variation in the RC and MP cells was measured separately, and the resulting distribution for both measurements was assumed to have a uniform distribution. For instance, the temperature variation for RC measurement is ranged from 295.9 K to 296.3 K, yielding that  $P_T$  ranged from 5015.12503 to 5015.28998 for R9e, from 5015.128395 to 5015.13457 for P7e, from 5015.124983 to 5015.29214 for R10e, and from 5015.128427 to 5015.13306 for P6e. The uncertainty of the temperature-dependent prefactor  $u(P_T)$  are then estimated to be  $7.69134 \times 10^{-25}$ ,  $3.89870 \times 10^{-25}$ ,  $8.26422 \times 10^{-25}$ , and  $2.58868 \times 10^{-25}$  cm<sup>-1</sup>/(molec·cm<sup>-2</sup>), respectively for each peak. The temperature variation of MP measurement was in a slightly different range from 295.2 K to 296.2 K., which corresponds to  $2.41165 \times 10^{-24}$ ,  $1.22241 \times 10^{-24}$ ,  $2.59128 \times 10^{-24}$ , and  $8.11664 \times 10^{-25}$  cm<sup>-1</sup>/(molec·cm<sup>-2</sup>) respectively for each peak. A combination of those with correction factor 4 (for averaging) indicates that  $u(P_T)$  is insignificant in RC and MP measurements (only about  $8.5 \times 10^{-4} \%$ ).

### *Uncertainty of length of the reference cell*

Mechanical measurements of the RC were performed using a caliper (resolution: 0.01 mm) that was calibrated against the national gauge block standards maintained by the KRISS. Thus, the uncertainty of the length of the RC  $L_{RC}$  was combined with the measurement and the uncertainty of the gauge block, resulting in  $20.01 \pm 0.05$  mm.

### *Uncertainty because of temperature and pressure measurements*

The temperature measurements were performed by attaching resistance thermometers to the cells. In addition, a pressure transducer was used to measure the MP absorption cells. The uncertainty contribution consists of the calibration certificate as a B-type and the repeatability of measurements as an A-type, which was calibrated against a standard platinum resistance thermometer (SPRT), and the pressure transducer was calibrated against a standard ultrasonic manometer in KRISS. Pressure gauges are traceable to the KRISS standards, whereas temperature sensors are traceable to NIST temperature fixed-point standards.

## **ST 3. Parametric evaluation of uncertainty of RE**

According to eq 4 of the main text, it was assumed that the major uncertainty source of radiative efficiency originated from the ACS measurement. It should be noted that the uncertainty of the radiative forcing (RF) model was unknown. This aspect of the uncertainty evaluation of RE might not be an issue for the comparison of RE values reported by independent research groups because the new narrow band model (nNBM) is currently considered the *de facto* standard of the RF model.<sup>6</sup> The uncertainty in the ACS measurement propagates to the final uncertainty of the radiative efficiency. The uncertainty of the ACS measurement is composed of the uncertainty due to temperature  $u(T)$ , pressure  $u(P)$ , certified reference material (CRM)  $u(x)$ , OPL of the multi pass cell  $u(L_{MP})$ , and wavenumber-dependent responsivity drift  $u_v(rd)$ . However, for  $u_v(rd)$ , the wavelength dependence did not significantly change the RE uncertainty, as discussed in the next section. According to the LUP, the combined relative standard uncertainty of the radiative efficiency can be estimated by:

$$ru^2(RE) = ru^2(L_{MP}) + ru^2(P) + ru^2(x) + ru^2(T) + 2 \cdot ru^2(rd) \quad (S9)$$

where  $ru$  is the relative standard uncertainty. Uncertainty due to pressure, temperature, and

CRM was evaluated in the same manner as in ST 2. For the uncertainty due to the OPL of the multi pass cell, the value was taken from the calibration result of the cell in accordance with the evaluation given in ST 2.

#### *Uncertainty of responsivity drift*

The instrumental responsivity drift was evaluated for a measurement period of 1.5 h, because the baseline ( $I_0$ ) fluctuated, as shown in Figure S2. Because the ACS measurement was not bracketed by consecutive single measurements of  $\Phi_0(\tilde{\nu})$ , the baseline of the ACS spectra fluctuated, affecting the iACS values. It was found that the probability distribution of the  $\Phi_{0,i}(\tilde{\nu})$  fluctuation in the measurement range of 500 – 3,000  $\text{cm}^{-1}$  was normal. The relative standard uncertainty of instrumental responsivity  $ru(rd)$  could be expressed as follows:

$$ru(rd) = \frac{\sqrt{\frac{\sum_{i=1}^n (R_{i,v}(\tilde{\nu}) - \bar{R}(\tilde{\nu}))^2}{n}}}{\bar{R}(\tilde{\nu})} \quad (\text{S10})$$

where  $n$  is the number of measurements 18 for 1.5 h, which covered the entire measurement procedure of each ACS, assuming that  $ru(rd)$  value was equivalent to that of iACS. This value was then combined as a B-type uncertainty with the standard uncertainty of the RE (eq S9). The center spike in Figure S2 originates from the water absorption in the spectrometer. However, this strong signature did not affect the RF value.



## Supplementary figures and tables

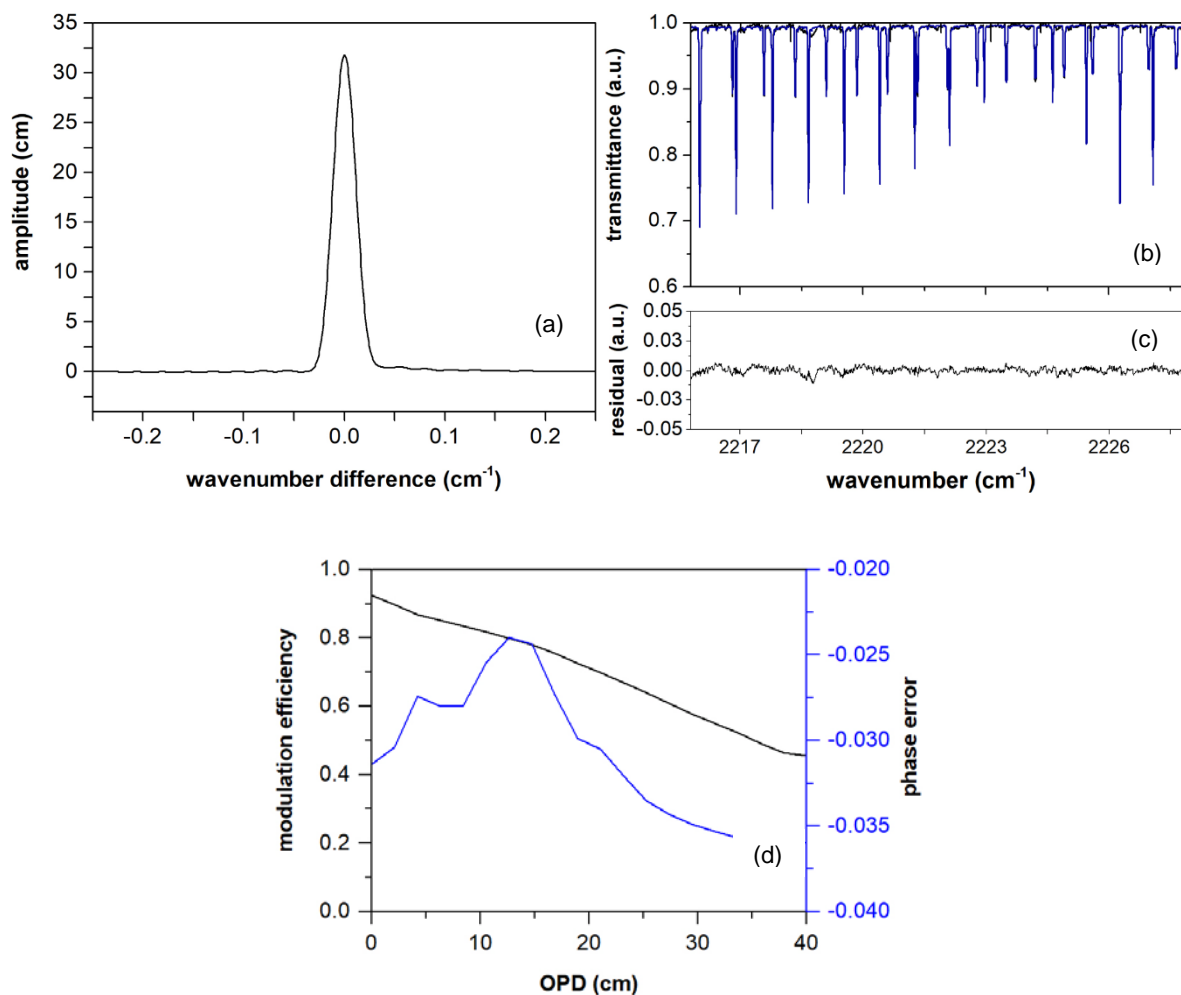


**Figure S1** ILS reconstruction results from the N<sub>2</sub>O spectrum. Reconstructed ILS (a) obtained using LINEFIT ver. 14 from the N<sub>2</sub>O spectrum with RC as measured by the HR-FTIR (b). A fit of column amount ( $4.6016 \times 10^{20} \text{ cm}^{-2}$ ) was superimposed with the measurement results in the wavelength range of 2215–2228 cm<sup>-1</sup>. Residuals are shown for the goodness of fit of the retrieved ILS (c). Phase error and modulation efficiency of the spectrometer (d).

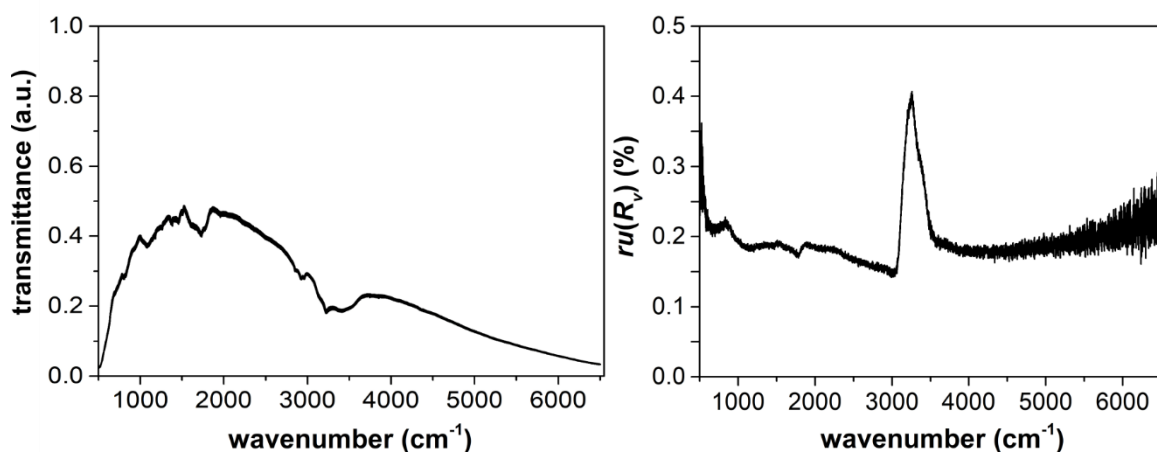


**Figure S2** Responsivity drift measurement. Transmittance stability measurement is shown for 1.5 h (left), associated with the relative standard uncertainty of responsivity drift (right). The drift variation in the uncertainty plot is shown at 3200 cm<sup>-1</sup>, which was caused by water vapor residues in the spectrometer body. However, the radiative forcing calculation model only considers the absorption band at 0 – 3,000 cm<sup>-1</sup>; the uncertainty spiking is not included in the uncertainty calculation.

**Table S1** Uncertainty budget of OPL calibration of MP. Values are displayed in relative (%).

Sources	Symbol	Relative Uncertainty (%), $k=1$	Sensitivity coefficient	DOF	Distribution	Type	Contribution (%)
Temperature of RC	$ru(T_{RC})$	0.19	-0.011	239	Uniform	A	2.4
Pressure of RC	$ru(P_{RC})$	0.14	0.034	4	Student's t	A	1.2
OPL of RC	$ru(L_{RC})$	0.12	160	99	Normal	A	0.9
Absorption (peak area) of RC	$ru(A_{RC})$	0.13	-110,000	705	Normal	A	0.8
Temperature of MP	$ru(T_{MP})$	0.19	0.011	239	Uniform	A	2.4
Partial pressure of N <sub>2</sub> O in MP cell <sup>1)</sup>	$ru(P_{MP})$	0.08	-0.7	4	Student's t	A	0.4
Absorption (peak area) of MP	$ru(A_{MP})$	1.2	14,000	449	Normal	A	91.9
Temperature dependent prefactor of MP <sup>2)</sup>	$ru(P_{T,MP})$	$4.92 \times 10^{-4}$	$-6.3 \times 10^{-4}$	$\infty$	Uniform	A	0
Temperature dependent prefactor of RC <sup>2)</sup>	$ru(P_{T,RC})$	$4.94 \times 10^{-4}$	$6.3 \times 10^{-4}$	$\infty$	Uniform	A	0
Combined uncertainty	$ru(L_{MP})$	1.3	-	25,701	Normal	-	100

1) Combined uncertainty of total pressure and amount of N<sub>2</sub>O in MP

2) The temperature-dependent pre-factor  $P_T$  (transition assignment) for each cell was 5015.20750 (R9e), 5015.13148 (P7e), 5015.20856 (R10e), 5015.13074 (P6e), 5030.48421 (R9e), 5030.66897 (P7e), 5030.74628 (R10e), and 5030.66823 (P6e) for the RC and MC, respectively.

**Table S2** Referred line data for OPL calibration of MP. Data were taken from the HITRAN 2016.

Isotopologue	$\nu$	$S$	$A$	$\gamma_{\text{air}}$	$\gamma_{\text{self}}$	$E''$	Transition	$J'$	$J''$
$^{14}\text{N}_2^{16}\text{O}$	2217.53281	$4.677 \times 10^{-20}$	97.31	0.0837	0.105	626.4924	R9e	10	9
$^{14}\text{N}_2^{16}\text{O}$	2217.74589	$6.330 \times 10^{-19}$	113.5	0.087	0.109	23.4641	P7e	6	7
$^{14}\text{N}_2^{16}\text{O}$	2218.29598	$4.959 \times 10^{-20}$	98.2	0.0824	0.104	634.8753	R10e	11	10
$^{14}\text{N}_2^{16}\text{O}$	2218.62524	$5.604 \times 10^{-19}$	115.5	0.0881	0.11	17.5982	P6e	5	6

**Table S3** Uncertainty budget of RE value of of NF<sub>3</sub>.

Sources	Symbol	Relative uncertainty (%), $k=1$	Sensitivity coefficient $i$	DOF	Distribution	Type	Contribution (%)
OPL of MP	$ru(L_{MP})$	1.3	$-6.2 \times 10^{-4}$	$\infty$	Normal	B	38.33
Pressure	$ru(P)$	0.047	$-5.5 \times 10^{-4}$	4	Student's t	A	0.05
Temperature	$ru(T)$	0.194	$6.6 \times 10^{-4}$	$\infty$	Uniform	A	0.93
Amount of substance	$ru(x)$	1.5	-2000	$\infty$	Normal	B	55.19
Responsivity drift	$ru(rd)$	0.474	17	$\infty$	Normal	B	5.51
Combined uncertainty	$ru(RE)$	2.02		$\infty$	Normal	-	100

**Table S4** Uncertainty budget of RE value of SF<sub>6</sub>.

Sources	Symbol	Relative uncertainty (%), $k=1$	Sensitivity coefficient <sub><i>i</i></sub>	DOF	Distribution	Type	Contribution (%)
OPL of MP	$ru(L_{MP})$	1.3	$-1.8 \times 10^{-3}$	$\infty$	Normal	B	85.06
Pressure	$ru(P)$	0.047	$-5.0 \times 10^{-3}$	4	Student's t	A	0.12
Temperature	$ru(T)$	0.194	$1.9 \times 10^{-3}$	$\infty$	Uniform	A	2.06
Amount of substance	$ru(x)$	0.10	-11,000	$\infty$	Normal	B	0.54
Responsivity drift	$ru(rd)$	0.474	100	$\infty$	Normal	B	12.22
Combined uncertainty	$ru(RE)$	1.36		$\infty$	Normal	-	100

**Table S5** Uncertainty budget of RE value of CF<sub>4</sub>.

Sources	Symbol	Relative uncertainty (%), $k=1$	Sensitivity coefficient $i$	DOF	Distribution	Type	Contribution (%)
OPL of MP	$ru(L_{MP})$	1.3	$-2.7 \times 10^{-4}$	$\infty$	Normal	B	85.41
Pressure	$ru(P)$	0.047	$-4.1 \times 10^{-4}$	4	Student's t	A	0.12
Temperature	$ru(T)$	0.194	$2.9 \times 10^{-4}$	$\infty$	Uniform	A	2.06
Amount of substance	$ru(x)$	0.05	-830	$\infty$	Normal	B	0.14
Responsivity drift	$ru(rd)$	0.474	28	$\infty$	Normal	B	12.27
Combined uncertainty	$ru(RE)$	1.35		$\infty$	Normal	-	100

**Table S6** Uncertainty budget of RE value of PMVE.

Sources	Symbol	Relative uncertainty (%), $k=1$	Sensitivity coefficient $i$	DOF	Distribution	Type	Contribution (%)
OPL of MP	$ru(L_{MP})$	1.3	$-1.0 \times 10^{-3}$	$\infty$	Normal	B	38.33
Pressure	$ru(P)$	0.047	$-7.0 \times 10^{-4}$	4	Student's t	A	0.05
Temperature	$ru(T)$	0.194	$1.1 \times 10^{-3}$	$\infty$	Uniform	A	0.93
Amount of substance	$ru(x)$	1.5	-3,300	$\infty$	Normal	B	55.19
Responsivity drift	$ru(rd)$	0.474	13	$\infty$	Normal	B	5.51
Combined uncertainty	$ru(RE)$	2.02		$\infty$	Normal	-	100



**Table S7** Uncertainty budget of RE value of PFMEE.

Sources	Symbol	Relative uncertainty (%), $k=1$	Sensitivity coefficient $i$	DOF	Distribution	Type	Contribution (%)
OPL of MP	$ru(L_{MP})$	1.3	$-1.7 \times 10^{-3}$	$\infty$	Normal	B	38.33
Pressure	$ru(P)$	0.047	$-7.1 \times 10^{-3}$	4	Student's t	A	0.05
Temperature	$ru(T)$	0.194	$1.8 \times 10^{-3}$	$\infty$	Uniform	A	0.93
Amount of substance	$ru(x)$	1.5	-1,100	$\infty$	Normal	B	55.19
Responsivity drift	$ru(rd)$	0.474	15	$\infty$	Normal	B	5.51
Combined uncertainty	$ru(RE)$	2.02		$\infty$	Normal	-	100

### Supplementary references

- (1) Abrarov, S. M.; Quine, B. M. *J. Math. Res.* **2015**, 2, 163-174.
- (2) Kim, Y.; Lim, J. S. *Bull. Kor. Chem. Soc.* **2020**, 41, 418-423.
- (3) Allen, M. G. *Meas. Sci. Techn.* **1998**, 9, 545.
- (4) BIPM.; IEC.; IFCC.; ILAC.; ISO.; IUPAC, IUPAP.; OIML. Evaluation of measurement data—guide for the expression of uncertainty in measurement. JCGM 100: 2008, JCGM 2008
- (5) Tellinghuisen, J.; *Anal. Chem.* **2019**, 91, 8715
- (6) Hodnebrog, Ø.; Aamaas, B.; Fuglestad, J. S.; Marston, G.; Myhre, G.; Nielsen, C. J.; Sandstad, M.; Shine, K. P.; Wallington, T. J. *Rev. Geophys.* **2020**, 58, e2019RG000691.